Rheo-NMR of Wormlike Micelles Formed from Nonionic Pluronic Surfactants

Bradley S. Douglass,[†] Ralph H. Colby,[‡] Louis A. Madsen,[§] and Paul T. Callaghan*[,†]

MacDiarmid Institute for Advanced Materials and Nanotechnology, School of Chemical and Physical Sciences, Victoria University of Wellington, Wellington, New Zealand, Department of Materials Science and Engineering, The Pennsylvania State University, University Park, Pennsylvania 16802, and Department of Chemistry, Virginia Polytechnic Institute and State University, Blacksburg, Virginia 24061

Received August 9, 2007; Revised Manuscript Received November 8, 2007

ABSTRACT: Using a range of techniques combining rheology and magnetic resonance, we here investigate the flow and alignment properties of wormlike micelles formed by a 5% w/w solution of the BASF difunctional block copolymer nonionic surfactant, Pluronic P105 in water along with 4.3% w/v 1-phenylethanol-d_5. A variety of shear-banding and alignment behaviors are observed, along with both stable and fluctuating flows. These strongly depend upon both temperature and applied shear rate. The deuterium-labelled alcohol enables study of alignment from quadrupole splitting, using a Hankel transform in the cylindrical geometry of our rheo-NMR cell.

I. Introduction

Wormlike micelles (WLMs) are long, threadlike assemblies of surfactant molecules in aqueous solution.[1−3] They constitute one of the many self-assembled micellar morphologies available to amphiphilic surfactants at concentrations above the critical micellar concentration (cmc). These structures include spherical micelles, cylindrical micelles, or more complex assemblies such as planar sheets and the sponge-like geometry of the L3 phase, the preferred state depending on the details of the surface curvature and free energy.[4−6] Those surfactant systems which form wormlike micelles (also known as threadlike micelles, rodlike micelles, or giant micelles) require a surface free energy condition which favors cylindrical curvature over rival states.[6] Generally, such systems include a co−surfactant or counterion. Canonical examples are the surfactant micellar systems CTAB (cetyltrimethylammonium bromide) in water[7] and CPyCl/NaSal (cetylpyridinium chloride/sodium salicylate) in water.[8,9]

In this article, we report on the properties of a very different system, formed by a nonionic triblock copolymer of poly(ethylene oxide)−poly(propylene oxide)−poly(ethylene oxide) (PEO−PPO−PEO) dispersed in water.[10−12] Such polymers are also known by the BASF trade name "Pluronic". Aqueous solutions of such triblock copolymers have been studied extensively, and are known to form spherical micelles.[11,12] In our system, the formation of WLM structures[13] is aided by the presence of the appropriate amount of an aromatic alcohol, 1-phenylethanol-d_5. Addition of a small quantity of aromatic alcohol expands both the core and corona of the spherical micelles,[13] presumably because the −OH hydrogen bonds to the ether oxygen of PPO (in the core) and PEO (in the corona). Once the right amount of hydrophobic alcohol is added, the system undergoes a structural change to WLMs, signified by $\sim 10^4$ increase in viscosity.

WLMs are of particular interest because of their peculiar rheological properties,[14,15] and in particular, their ability to exhibit "shear-banding" in which two different viscosity states of the same solution can coexist.[16−20] We shall show here that WLM phases of Pluronic surfactants do indeed exhibit shear banding, but that complex and subtle variants of both shear-banded flow and molecular ordering are apparent. These variants are shown to depend strongly on the external variables of temperature and applied shear rate. While the detailed structure of nonionic WLMs is the subject of speculation, we will find it helpful to present the schematic shown in Figure 1 in order to show the separation of length scales between entangled micelles, local cylindrical structure, and triblock copolymer structure.

The origin of shear-banded flow in such complex fluids can be explained by a stress−strain rate constitutive relationship.[21−24] In particular, a region of declining stress with increasing shear rate is inherently unstable and leads to coexistence of flow in separate rising stress branches, as required to satisfy the overall rate of strain condition.[16] The measured flow curve, under controlled strain-rate conditions, will be characterized by a stress plateau in which different proportions of the low and high strain-rate phases are determined by a lever rule, as the average strain rate is swept. The origins of a declining stress branch in the stress/strain-rate constitutive relation is believed to be associated with the formation of shear-induced structures.[25] For example, in the reptation theory of monodisperse polymers, at shear rates exceeding the tube disengagement rate, polymer orientation leads to strong shear thinning of the viscosity.[21] The constitutive behavior of semidilute solutions of WLMs is also believed to be governed by reptation dynamics in concert with dissociation/recombination processes. Hence, WLMs are often known as living polymers or equilibrium polymers.[14,25,27] Most WLMs exhibit a nonmonotonic flow curve, following the schematic example shown in ref 16. At low shear rates, the flow curve is Newtonian. At higher shear rates, shear thinning behavior may be found, while above a critical shear stress/strain there

* Corresponding author. E-mail: paul.callaghan@vuw.ac.nz.
[†] MacDiarmid Institute for Advanced Materials and Nanotechnology, School of Chemical and Physical Sciences, Victoria University of Wellington.
[‡] Department of Materials Science and Engineering, The Pennsylvania State University.
[§] Department of Chemistry, Virginia Polytechnic Institute and State University.

10.1021/ma071807f CCC: $40.75
Published on Web 01/08/2008

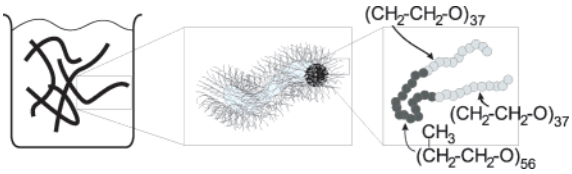

Figure 1. By means of small-angle neutron scattering data, the addition of the stabilizing hydrophobic 1-phenylethanol to a P105 in water solution is thought to generate wormlike micelles, filaments which are somewhat "hairy" due to the more hydrophilic poly(ethylene oxide) component of the copolymer comprising the micelle corona. On the basis of neutron scattering measurements, the radial extents of both "core" and "corona" are ~30 Å.[13]

often exists a stress plateau that can extend for decades of shear rate.

Shear banding in the stress plateau region has been convincingly demonstrated by techniques as diverse as nuclear magnetic resonance (NMR) velocimetry,[20,29,30] laser Doppler velocimetry (LDV),[31] dynamic light scattering,[32−35] and ultrasonic velocimetry.[36−38] That shear banding, in systems close to the isotropic-to-nematic (I−N) phase transition, may be associated with coexisting states of different orientational order, is suggested by birefringence,[7,17,18] NMR spectroscopy,[39] and small-angle neutron scattering (SANS).[40] In many of these studies, shear-banded flow has been associated with shear-induced phase transitions, wall slip, and shear stress fluctuations.

In this paper, we first present the phenomenological rheology data on Pluronic P105/phenylethanol WLMs exhibiting some unusual behavior, including two maxima in the temperature dependence of apparent viscosity at high shear rates. We then show how rheo-NMR, specifically ^{2}H NMR splittings indicative of alignment, can be used to help understand the rheological observations.

II. Rheology of Wormlike Micelles

Surfactant/co-surfactant systems exhibiting wormlike micellar behavior have three principal rheological characteristics. First, there exists a region of the phase diagram (in which the proportions of surfactant and co−surfactant are adjusted), where there is a significant increase in zero shear (or low shear) viscosity. This viscous phase is generally associated with the formation of long threadlike micelles whose dynamics are dominated by the interplay between reptation and dissociation-recombination. This is the semidilute regime of wormlike micelles. Second, the linear rheology of such semidilute WLMs[26] is characteristic of a Maxwell fluid, exhibiting a semicircular Cole−Cole plot. At high frequencies, deviation from simple Maxwell behavior is associated with dissociation-recombination processes. A characteristic feature of wormlike micellar nonlinear rheology is the presence of a plateau on the flow curve, generally associated with the sub-division of the material into coexisting low and high shear rate phases, a manifestation of shear banding. Furthermore, this shear-banded state is often associated with strong fluctuations. Stress oscillations have been found for a variety of micelle systems[40−49] and are sometimes associated with the growth and destruction of the shear-induced structures, in shear thickening systems. Stress fluctuations may be purely periodical or suggestive of chaos.[46−48] Recently Fielding and Olmsted have shown that such instability may be a consequence of coupling of the hydrodynamics to a strain-rate dependent micellar variable, such as micelle length or concentration.[50,51] Experiments have been unable to elucidate the origin of instabilities, although in velocimetry studies, fluctuating wall slip has been shown to play a significant role.[38,47,48]

The strategy behind the present study is to compare rheometric and rheo-NMR properties of a particular Pluronic/phenylethanol phase, specifically one which has been selected due to its exhibition of a significantly enhanced low shear viscosity, and because neutron diffraction data is consistent with scattering from threadlike objects. The existence of this viscous phase is highly temperature dependent, so that temperature is an important parameter of the study. We examine both the linear viscoelastic behavior, as well as the flow curve, taking care to elucidate time dependence in the stress. This is of particular importance in the present system because of the existence of slow (e.g., ~100−1000 s) time scales in the rheological behavior. We find that fluctuations play a role in this system, and that dynamics depend sensitively on both shear rate and temperature. Thus, this study focuses on shear rate and temperature as the primary variables.

III. Background to Rheo-NMR

In its simplest guise, rheo-NMR[52−56] comprises the study of spectroscopic properties of complex fluids during deformation within the magnet and rf coil of an NMR spectrometer. However, a more effective approach is to use the spatial localization tools afforded by NMR imaging (MRI). Thus, an obvious advantage of rheo-NMR is that it may be used to image the velocity field within a rheological cell, thus providing noninvasive insight concerning the exact nature of deformational flow.[55] The key to this approach is the use of NMR imaging at microscopic resolution,[54] since the containment cells are often of millimeter length scale. However, if one wishes to examine molecular properties via NMR spectroscopy, then the same image localization methods may be used to study NMR spectra at different positions in a heterogeneous flow. Hence rheo-NMR has a dual focus on NMR microscopy and NMR spectroscopy, the former giving insight at the mechanical length scale (>10 μm) and the latter at the molecular length scale. By the use of deuterium labeling, it is possible to employ the deuterium quadrupole interaction to measure local order, since this interaction results in a two line NMR spectrum in which the splitting is proportional to the local order parameter and to the alignment with respect to the magnetic field.

A. Geometry and Apparatus. Figure 2 shows the Couette cell used for all rheo-NMR measurements described herein. In the limit of small gap spacing relative to cell radius, this approximates infinite planes sheared relative to each other. The maximum shear rate in the cell gap, seen at the inner wall of the gap, is given by the linear speed of the inner cylinder wall divided by the gap spacing. The physical cell consists of two concentric glass NMR tubes—a 10.0 mm o.d., 9.0 mm i.d. tube enclosing a 7.5 mm o.d. tube—separated by Teflon spacers to maintain a fixed gap between the tubes. When imaging the velocity of samples in the gap, vibration and nonconcentricity of the tubes become a critical issue. Thus, we use spacers near the top and in the middle of the tube gap, and ensure that the outer tube is held rigidly in the rf coil using Teflon spacers, o-rings, and often a thin layer of Teflon tape wound around the outer tube.

B. Spectroscopy. In order to assess the bulk average orientational order induced in the sample by shear, we have used deuterium NMR spectroscopy[57−59] on ring-labeled 1-phenylethanol-d_5 molecules. These molecules act as local probes of order via their spatially anisotropic interactions (librations and collisions) with the WLM matrix.[60] During the time scale

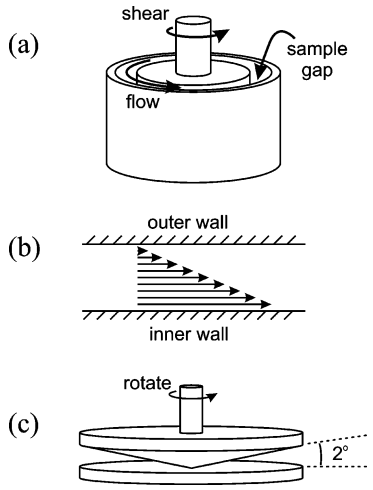

Figure 2. Rheo-NMR sample cell. Part (a) depicts a shear cell in a Couette geometry (concentric cylinders), which is placed inside an NMR spectrometer for rheo-NMR measurements. The inner cylinder is rotated using a stepper motor outside the magnet via a coupling driveshaft, while the outer cylinder remains fixed relative to the magnet. The flow (velocity) across the gap is imaged to provide the flow map shown in part (b) as a function of position in the gap. Molecular information via NMR spectroscopy is also obtained on the sheared solution. Part (c) shows the cone-and-plate shear cell geometry used in the conventional rheology studies described in section IV A below. Here the sample is sheared between a flat surface and a rotating inverted cone.

of the deuterium quadrupole interaction ($\sim 1/10^5$ Hz), the picosecond movements of the probe molecules interact $\sim 10^6$ times with their local environment, producing a time average of the motions for each individual molecule. Each of the $\sim 10^{21}$ probe molecules in the sample then average spatially to give the full superposition ^{2}H NMR spectrum. Thus, these deuterated probe molecules "inherit" the order of the host matrix and the measured deuterium NMR spectrum exhibits a splitting proportional to the average order in the sample,[61−63] which in our system is induced by shear. Consistent with our NMR observations, and with neutron scattering measurements,[13] we suppose that the phenylethanol probe molecule resides within the core of the WLMs, and that the ^{2}H NMR splitting reflects the overall alignment of the WLM tubes along the shear direction. The spatial associations of these molecules in the WLM solution will be discussed in further detail in section V D.

When the probe molecules reside in an isotropic phase of the material, the deuterium NMR spectrum consists of a single unsplit peak. For a single ordered phase, with only one average orientation of the C−D bonds with respect to the magnetic field, we see one spectral splitting (a doublet). One may simply use a single 90° RF (pulse-acquire) pulse sequence (see Figure 3a) to measure this splitting, as we used in the spectroscopy experiments shown in Figure 6. Because the pulse-acquire sequence used to acquire the quadrupole splitting data shown below in Figure 6 measures signals on the ∼1 s time scale, a resolution on the order of 1 Hz is in principle possible.

When a system generates two or more phases in which the probe molecules may exist, which happens for our WLM system when we have greater than 3 wt % phenylethanol, spectra from each phase appear superposed. For a coexisting isotropic and ordered phase the split spectrum of the ordered phenylethanol would be superimposed on the (single peak) spectrum of the isotropic phase. Note that such a single peak spectrum may be removed by use of a double quantum filter (DQF) pulse sequence that refocuses the quadrupole interaction while dropping the isotropic peak from the observed spectrum.[64] In the

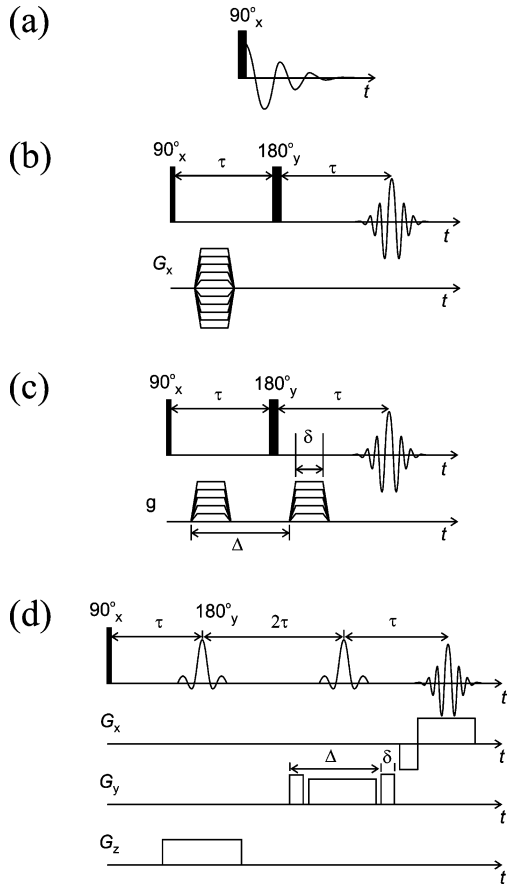

Figure 3. (a) Basic NMR pulse program resulting in a free induction decay signal. (b) Projection profile experiment, generating a 1D Cartesian image able to be transformed to a radial space 1D image (c) PGSE experiment, the decay of signal strength at increasing gradient strengths g revealing a mean squared displacement. (d) Pulse program designed to obtain an image of flow in the velocity direction of the Couette cell as a function of the velocity gradient direction, where slice-selection has taken place in the velocity and vorticity directions.

results we present, two different splittings are observed simultaneously, corresponding to deuterons in coexisting, but differently ordered, phases. That these are both ordered phases we are able to show by means of an $90^\circ_x - t - 180^\circ_y - t -$acquire echo experiment, which has the effect of refocusing magnetic inhomogeneity but leaving the quadrupole interaction unscathed. Any quadrupole interaction resulting from ordered phases should then be apparent in both the evolution (t) and acquisition dimensions.

C. (Radial) Spectroscopic Imaging. To observe spatial variations in the shear-induced orientational order across the cell gap, we use the pulse sequence shown in Figure 3b for NMR spectroscopic imaging. In contrast to the pulse-acquire experiments described above, which measure the gap-averaged orientational order, the spectroscopic imaging approach enables us to spatially correlate the dependence of shear-induced deuterium spectral splitting with the local shear rate at a given gap position. This facilitates the direct comparison of shear banding and fluctuations obtained using velocimetry with the molecular order present in the sheared solution.

By introducing a purposefully constructed linear magnetic field gradient—which adds to, or subtracts from the applied magnetic field—spatial information can be obtained about a sample in an NMR experiment. It is well-known[54] that a so-called "projection profile" can be obtained (i.e., a 1D image), the intensity of which is simply an integral (over the plane

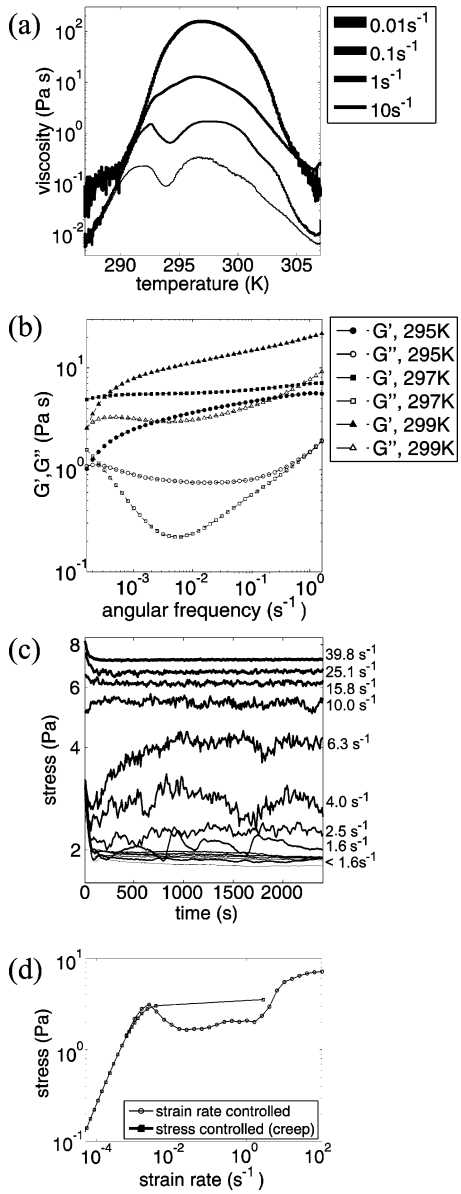

Figure 4. (a) Shear viscosity of the Pluronic wormlike micelle solution, obtained at various shear rates, including close to zero shear. (b) Linear rheology of the P105 solution showing a crossover of G' and G'' at 1.6 $\times$ 10^{-4} s^{-1} or lower, indicating a terminal relaxation time of ~1000 s. The upturn of G'' at 297 K occurs at ~5 $\times$ 10^{-3} s^{-1}, potentially indicating a breakage/recombination time for the micelle of around 200 s, and hence a reptation time of ~5000 s. (c) Transient stress response to shear startup, at 297 K. Stress fluctuations are visible between 1.58 and 6.3 s^{-1} (d) Nonlinear rheological flow curve of the material at 297 K, using both stress- and strain-controlled modes of rheometry.

perpendicular to the field gradient) of the spin density as a function of the spatial direction in which the gradient lies. Although any NMR spectroscopic technique may be combined with an imaging sequence in a typical pulse program, only the relevant aspects of deuteron spectroscopy within an assumed cylindrically symmetric flow field will be discussed here. The cylindrical symmetry affords benefits in experimental time and simplicity which are both desirable and at times vital to the feasibility of the experiment.

In general, a 1D projection is insufficient to map the sample spin density over a 2D plane, leading to the use of standard two-gradient imaging sequences. However, in the case of a known cylindrically symmetric distribution of signal, the image may be reconstructed by performing the radial 1D

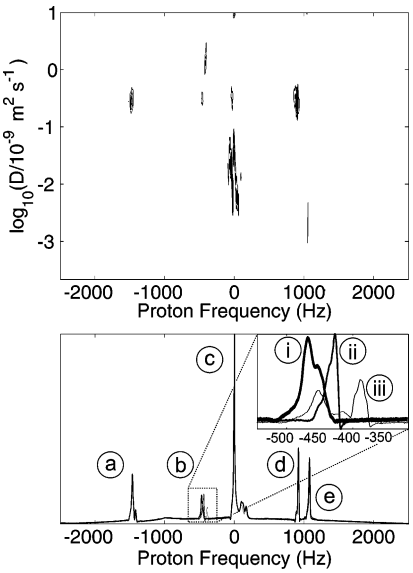

Figure 5. Proton NMR spectrum of the Pluronic wormlike micelle solution (below) and the DOSY spectrum resolving the diffusion properties of each spectral line (above). These lead to the following peak assignments: (a) C_6H_5 (phenylethanol); (b) CH (phenylethanol) in addition to HDO at three temperatures, (i) 282, (ii) 293, and (iii) 307 K; (c) $O-CH_2$ (PEO, PPO); (d) CH_3 (phenylethanol); (e) CH_3 (PPO).

Fourier transformation (the Hankel transformation) on the reciprocal-space data obtained in the projection profile experiment.

The Hankel transformation is an integral transformation using the Bessel function of order zero J_0 as the kernel, and can be easily derived from the well-known 2D Fourier variant by a simple expression of the two Cartesian variables (x,y) in terms of their cylindrical counterparts (r,θ), resulting in the form

$$\rho(r) = H[S(k)] = 2\pi \int_0^\infty S(k)J_0(kr)k \, dk \qquad (1)$$

To collect the k-space signal $S(k)$, the 1D k-space is traversed by the imposition of a pulsed magnetic field gradient in the time intervening the 90° excitation pulse and the 180° refocusing pulse of a spin echo experiment. The geometry of the required image is controlled by parameters such as the gradient pulse duration, gradient step size and the extremal gradient values. Where the maximum gradient is applied (the point farthest out in k-space), the minimum pulse duration may be applied, to obtain a minimal echo time, reduce signal loss due to irreversible relaxation, and decrease the experimental time over which spins may undergo undesirable diffusion or flow.

D. Diffusion NMR. Magnetic field gradients in NMR may also be used to obtain diffusion information. In particular the use of the pulsed-gradient spin echo (PGSE) technique allows measurement of phase changes associated with the displacement of an ensemble of sample nuclei over a well-defined time period.[54,65] With this technique, a pair of magnetic field gradient pulses surrounding a simple Hahn echo 180° rf pulse causes the phase acquired by a spin ensemble prior to the pulse to be negated during the field gradient pulse after the rf pulse, under the condition of zero motion. Should the ensemble undergo diffusive motion, dephasing will occur, and the vector addition of such a dephased ensemble produces an attenuated NMR signal.

The pair of field gradient pulses can be characterized by their duration δ, amplitude g, and the time between them Δ (see Figure 3c). The degree of signal attenuation directly correlates

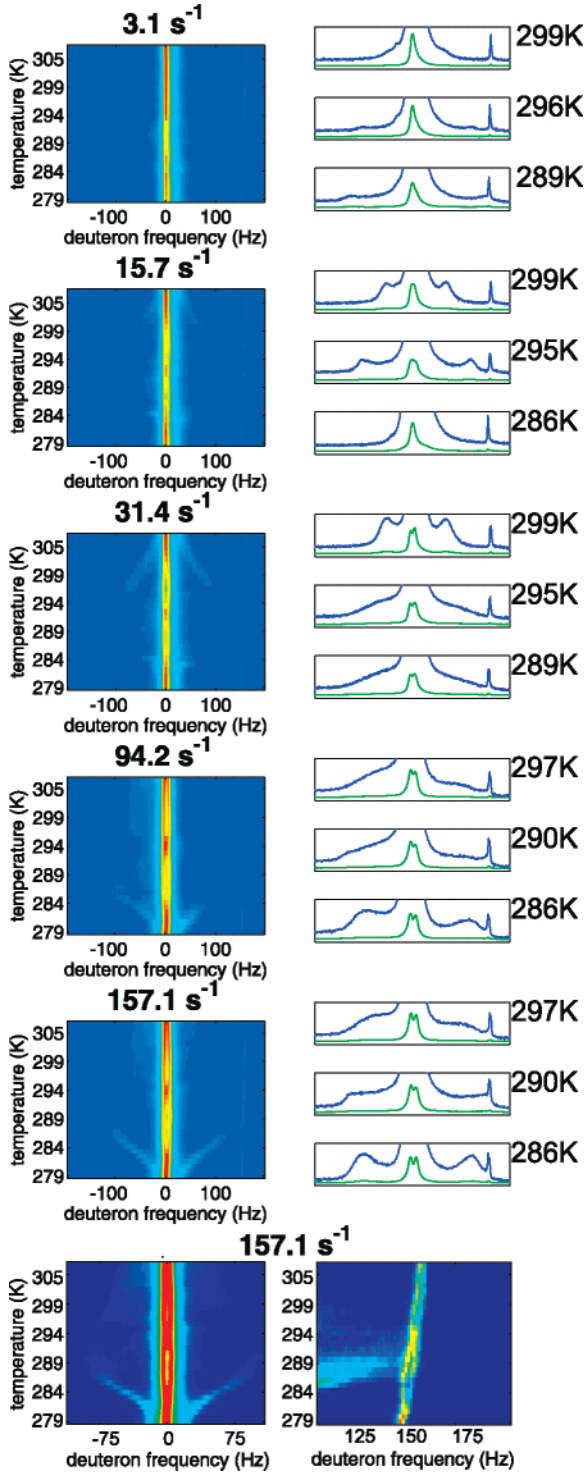

Figure 6. Deuterium NMR spectrum as a function of temperature at five shear rates shown in the five top left panes, with 1D spectra extracted at three different temperatures for each on the right. These 1D spectra are shown at full intensity range, as well as enlarged by a factor of 20, to show less intense features.

with the distance traveled by the molecules. The residual phase acquired by spins in a time t can be denoted $\phi(t)$ and the attenuation of the normalized echo signal will then be the average over the whole spin ensemble, given by

$$E(t) = \langle \exp[i\phi(t)] \rangle \tag{2}$$

which in the case of ordinary unrestricted diffusion is equal to the Stejskal−Tanner relation[65]

$$E(g,\delta,\Delta) = \exp\left\{-\gamma^2 g^2 D \delta^3 \left(\frac{\Delta}{\delta} - \frac{1}{3}\right)\right\} \tag{3}$$

By fitting such attenuation factor data at varying values of those crucial parameters, a diffusion coefficient D may be extracted. In this work we vary only the gradient strength g at fixed δ and Δ.

In practice, each spectral component of an NMR experiment can be correlated with a different diffusion coefficient, providing a 2D DOSY spectrum,[66] and hence a means of associating spectral features with components of the sample which diffuse at different rates. This is particularly helpful in identifying molecular species since the diffusion coefficient is related to molecular or subdomain size through the use of the Stokes−Einstein relation of kinetic theory.

E. NMR Velocimetry. As depicted in Figure 2, we also perform velocimetry measurements in the Couette geometry to assess nonlinear rheological flows such as shear banding. The pulse sequence used for this NMR experiment is shown in Figure 3d. Here we encode 1D velocity images of a slice perpendicular to the Couette cell axis to spatially resolve the fluid velocities in the gap to a resolution of ~30 μm. Since we accomplish the image encoding in 1D only (along the "read" direction), these images require only ~1 s per repetition, which enables the resolution of fluctuations in flow velocities on this time scale. We note that for a Newtonian fluid sheared between infinite planes, the velocity will depend linearly on the gap position, while in our Couette geometry the velocity dependence has some curvature due to the deviation from planarity and finite gap thickness, creating a mild variation in stress across the gap. We will discuss this further in conjunction with our velocimetry data on the WLM solution below.

Under application of a linearly varying magnetic field (a field gradient G) across a sample dimension x, the local spin precession frequency at Cartesian position x in our sample cell varies as

$$\omega(x) = \gamma B_0 + \gamma G \cdot x \tag{4}$$

where B_0 is the homogeneous polarizing field and γ is the gyromagnetic ratio of the nucleus of interest. The local precession frequency of nuclear subspecies is then measured by the rf detection coil as[54]

$$S(k) = \rho(x) \exp(2\pi i k \cdot x)\, dx \tag{5}$$

where $\rho(x)$ is the local spin density and k belongs to the Fourier space reciprocal to x, given by $2\pi^{-1}\gamma G t$, and t is the time of evolution during application of the magnetic field gradient.

In order to encode velocities into NMR signals, we again incorporate the PGSE feature described in section III D into our experiment,[65] as shown in Figure 3d. Field gradient pulses prior to and after the 180° rf "echo" pulse cause the spins to acquire a position-dependent phase at these two distinct times and thus encode velocity information. The velocity and position-modulated signal is given by

$$S(k,q) = \int \rho(x) \left[\int \bar{P}_s(Y,\Delta) \exp(2\pi i q \cdot Y) dY\right] \exp(2\pi i k \cdot x)\, dx \tag{6}$$

where q is the variable in the reciprocal space of velocity ("q-space"). Double inverse Fourier transformation of S yields the average propagator located at position (pixel) x of the sample. This propagator shows both the mean flow at a localized region

of the sample as well as its variance. We thus image the velocity profile across the gap of a Couette cell of a sheared sample.

Note that in practice the q gradient pulses used in velocity-encoding are applied in one Cartesian direction, and hence an additional slice-selection is required so as to observe only spins with velocities collinear with the magnetic field gradient g. That is, those spins with velocities appreciably off the axis of g are excluded from the volume of sample imaged.

The experimental time required to obtain an image of $v(r)$ depends on the velocimetric and spatial resolution required. For example, to resolve a sample velocity to approximately 10 μm s^{-1} and map at a spatial resolution $\sim$100 μm requires an experimental time of about 10 min. We must also design our data acquisition sequences to ensure that a minimum of fluid is displaced into adjoining pixels within the experimental time delays (Δ, etc.).

IV. Experimental Section

A. Sample Preparation and Rheometry. The wormlike micelle solution used in this study is composed of a solution of 5% w/w of the BASF Pluronic P105 in H_2O, to which, per 5 mL of Pluronic solution, 0.213 g of 1-phenylethanol-d_5 (Cambridge Isotopes) was added.

The rheometer used is a stress-controlled TA Instruments AR2000. This instrument can be operated in a strain-controlled manner via an internal feedback loop. Both modes are used to verify the validity of obtained data and to extend the angular frequency and shear rate ranges over which data are acquired. In particular, at lower angular frequencies, strain rates otherwise unachievable are mapped as a function of stress through creep measurements in which a constant stress is maintained during which deformation occurs. Various geometries are available for this system, such as the Couette geometry and the cone-and-plate geometry, both shown above in Figure 2.

Several logistical constraints limit the range of frequency and shear rates studied. Two primary considerations are the minimum measurable torque, which restricts measurements at low frequency and low shear rate, and sample ejection and/or inertial effects at high shear rates which can be problematic in the cone-and-plate geometry. The shear-rate range covered in this work is from 0.01 s^{-1} up to a maximum of 10 s^{-1}.

Temperature is controlled via the flow of water past a Peltier element located at the base of the rheometer cell used. A Type T thermocouple in thermal contact with the plate surface is also installed to calibrate with the NMR experimental temperature, as described in the next section.

B. Magnetic Resonance. Our work uses a custom rheo-NMR system utilizing a stepper motor located atop a Bruker Avance 400 MHz wide bore magnet. This motor and associated gearbox transfers torque to a Couette cell located within the sample bore via a drive-shaft. The Couette cell is a concentric-cylinder system composed of two standard glass NMR tubes separated by Teflon bearings, with a bayonet head on the inner cylinder to couple with the drive shaft. A gap of 0.75 mm is generated between the two cylinders where the outer diameter of the inner cylinder is 7.5 mm; the inner diameter of the outer cylinder is 9.0 mm—a geometry which results in conversion from rotation frequency to an average shear rate equal to the inner wall velocity divided by the gap width, which for a 1 Hz rotation frequency of the inner cylinder is

$$\dot{\gamma} = \frac{7.5\pi \text{ mm s}^{-1}}{0.75 \text{ mm}} = 10\pi \text{ s}^{-1} = 31 \text{ s}^{-1} \qquad (7)$$

The maximum practical shear rate is approximately 200 s^{-1}, limited by signal disturbances due to physical vibration of the sample tubes during rotation.

The NMR microimaging studies utilize a Bruker Micro2.5 triple-axis gradient probe for which the currents driving the magnetic field gradients, G, are generated by a Bruker GREAT40 current supply. Gradients are variable up to a maximum possible strength of 96 G cm^{-1}.

NMR temperature control is performed through a Type T thermocouple attached to a Bruker BVT2000 control unit, which feeds back on heating coil current and air flow to maintain the desired temperature. We note that the thermocouple tip lies approximately 30 mm below the active region of the rf coil used in the experiment. In order to calibrate temperature with the rheometer to within 1 K, we also use a portable Type T thermocouple with its tip at the sample center.

V. Results

A. Rheometry. Figure 4a shows the dependence of viscosity on temperature of the Pluronic micellar solution, at a range of low shear rates. The $\sim 10^4$ increase in low shear rate viscosity can only mean that we have formed WLMs long enough to entangle at this concentration. Remarkably, the region of high viscosity is rather small, covering a temperature range of only 15 deg (from $\sim$290 to $\sim$305 K), although this is extended a small amount with increasing shear rate. At shear rates >0.1 s^{-1}, a local minimum in the temperature dependence of viscosity is seen, at 294 K, in the midst of the WLM temperature regime! This might arise from our worms becoming sufficiently long to either form a nematic phase at high rates or break at high rates. We find that this local minimum is mirrored in shear-dependent NMR spectroscopic properties of the WLM solution.

The linear viscoelastic response of the WLM solution is shown in Figure 4b. These data are also indicative of a highly entangled WLM solution. At low frequencies, behavior typical of a Maxwell fluid is found, while at higher frequencies strong deviations from Maxwell behavior are observed. Note however that the angular frequency $\sim 5 \times 10^{-3}$ s^{-1} at which this break from Maxwellian behavior is found is relatively low when compared with other WLM solutions, and may thus be consistent with a very slow WLM dissociation rate. This immediately raises the question of thixotropy and the need to allow for time dependence in rheological measurements of the nonlinear viscosity. Thus, we show in Figure 4c time dependent stress measurements over a range of shear rates. Here characteristic relaxation times of up to $\sim$500 s are found before a stress plateau is reached. Consequently, we take special care in establishing the flow curve for this material. Figure 4d shows a flow curve composed of a strain-rate-controlled measurement, in addition to a stress-controlled creep measurement made to measure sufficiently low strain rates to demonstrate the Newtonian region of the material. Of particular note is the coincidence of the lowest shear rate showing temporal stress fluctuations at 1.58 s^{-1} (Figure 4c), and the shift of the flow curve into the high-shear-rate branch (Figure 4d).

B. ^{1}H Spectrometry and Diffusometry. Figure 5 shows the 400 MHz proton NMR spectra obtained from the Pluronic WLM system in D_2O at three different temperatures, 282, 293, and 307 K. Note the temperature dependence of the HDO/OH peak in the vicinity of -1.25 ppm (all chemical shifts here are presented relative to the $O-CH_2$ line), superposed on a temperature-independent CH group from the phenylethanol. The upper part of the figure shows the intensity of the peaks as a function of field gradient strength in a PGSE experiment. The most rapid decay in intensity corresponds to the fastest diffusing molecules. The HDO peak exhibits the fastest molecular diffusion rate, while the phenyl alcohol aromatic ring and methyl groups are also easily identified at -3.625 and $+2.4$ ppm, respectively, with respect to the Pluronic $O-CH_2$ line. At 0 ppm and $+2.625$ ppm we observe peaks associated with

extremely small diffusion rates, which we assign respectively to the poly(ethylene oxide) and poly(propylene oxide) CH_2 and poly(propylene oxide) methyl groups on the Pluronic surfactant chains of the micelles.

When we inspect the deuterium NMR spectrum for samples of the Pluronic WLM system in H_2O, we observe a weak signal at 2.5 ppm upfield of the aromatic deuterons of the phenylethanol. We thus attribute this weak signal to HDO deuterons at natural abundance, an identification confirmed by the intensity ratio of this peak to that of the aromatic deuterons. Second, the temperature dependence of the HDO peak provides a useful internal calibration for temperature.

C. Deuterium NMR Spectroscopy. Our first NMR examination of shear-dependent behavior consists of a deuterium NMR study of molecular ordering, probed via splittings of the phenylethanol deuterium peaks. Their signal results from all fluid in the gap, and thus represents the average degree of order in the cell. We show in Figure 6 a series of temperature and shear-rate regimes, in which a finite order parameter is demonstrated. That this is a quadrupolar interaction, is indicated by both double-quantum filter and 2D Hahn echo experiments in which the bilinear nature of the quadrupolar interaction is apparent.

The existence of two splittings is a curious aspect of this work and a feature seen through much of this study. We discuss our interpretation of this phenomenon in section VI. Here we present the range of observed spectral behaviors. Figure 4 shows ^{2}H NMR spectra obtained over a range of temperatures (279 to 308 K) and shear rates 3.1 to 157.1 s^{-1}. These are presented as two-dimensional color plots with the color representing the intensity of the ^{2}H NMR peaks. Also shown are selected spectral slices at various temperatures. Some particular features of the spectra are noteworthy. First, we note that the dominant peak, centered at 0 Hz corresponds to the deuterated aromatic ring of the phenylethanol. At 4.6 ppm upfield can be found a weak ^{2}H NMR peak associated with the residual natural abundance deuterons in the water solvent. Note that the frequency of this peak is strongly temperature dependent, as described in section V B. Second, we note that the aromatic peak is split, indicating molecular ordering, over particular bands of temperature, and that the splitting is dual in nature, with the greatest peak intensity associated with a narrow splitting of around 20 Hz, and a much weaker component whose splitting is much larger, varying strongly with temperature to values up to 200 Hz. This outer peak splitting is well-defined at the higher end of the temperature range when the shear rate is low and even at the lowest shear rate of 3.1 s^{-1}, but changes become well-defined at lower temperatures only when the shear rate increases above 40 s^{-1}.

In the vicinity of 294 K, the dominant peak splitting disappears for all shear rates. This null in the dominant peak splitting is not clearly mirrored in the weak outer splitting, which instead seems to exhibit a state in which the order parameter is ill defined. We note that a similar inflection is seen in the low shear viscosity data, also at 294 K.

D. Spatially Resolved Velocimetry. We now turn to rheo-NMR measurements in which imaging is used to spatially localize the properties of the fluid across the gap. First we focus on NMR velocimetry. At flow startup the velocity profile exhibits a near-Newtonian profile, evolving over a period of a few minutes to a steady state in which strongly non-Newtonian behaviors are apparent. This effect is illustrated in Figure 7, where we show a succession of velocity profiles, separated in time by 60 s, at an exemplary temperature of 304 K and shear rate of 6.2 s^{-1}. Note that steady state behavior in this case is achieved after a period of approximately 10 min, or slightly longer, which is in excellent agreement with the transient stress response for the shear rate of 6.3 s^{-1} shown in Figure 4c. In all subsequent data, the fluid was driven in steady shear for a time sufficient (>10 min) for the fluid velocity to reach such a steady state.

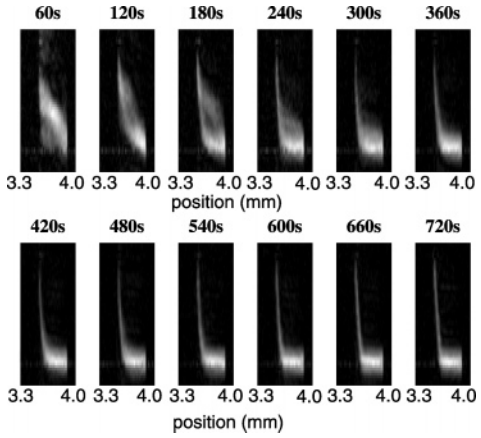

Figure 7. Time series of velocity maps shown for a single shear rate, 6.2 s^{-1}, at a single temperature, 304 K. The times indicated are relative to the time at which the shear rate was stepped from zero; a terminal shear rate profile can be seen after 600−700 s.

Similar to the above ^{2}H NMR measurements of molecular ordering, the fluid velocity profiles shown in Figure 8 are strongly temperature and shear-rate dependent. We present, for simplicity, two canonical examples, in which shear rates are swept over the entire range of interest, at temperatures of 293 and 304 K. In each case we measure a preselected diametral slice of width 1 mm (along the velocity direction) and depth 5 mm (along the cell axis) taken across the Couette cell. The signal data are shown as two-dimensional grayscale maps in which the horizontal dimension is the radial position across the Couette cell, while the vertical dimension is the fluid velocity, calculated from the measured displacement over the encoding times Δ used in each case, ranging from 9 up to 48 ms. The vertical bar shows the expected broadening of displacements resulting from diffusion alone. Broadening beyond that range therefore corresponds to velocity fluctuations.

Figure 8 shows the case of 293 K, in which a range of different shear profile behaviors is exhibited. At the lowest shear rate, 3.1 s^{-1}, shear banded flow is apparent. At higher rates, in the range 6.3−62.8 s^{-1}, fluctuations are seen, and banding consists of a high shear region both at the inner wall and the outer wall of the gap. Above 62.8 s^{-1}, the banding disappears and the flow returns to near-Newtonian character, although fluctuations still play a role. Figure 9 shows shear rate profiles for the case of 304 K. Here, a well-defined shear band is demonstrated at low shear rates (up to 12.6 s^{-1}), then a transition through unstable flow to near-Newtonian behavior above 25 s^{-1}. The inward curvature at highest shear rates results from azimuthal movement of the fluid near the inner wall, over the times taken (between 1.6 and 5 ms) to encode for transverse spatial position.

E. Spatially Resolved Spectroscopy. We now turn our attention to the spatial localization of molecular ordering. In this case we use the Hankel transformation method, described in section III C, to produce a radial image of the ^{2}H NMR spectrum. Figures 10 and 11 compare the spectral and velocity profile images. Spectroscopic images are presented as two-dimensional grayscale plots with the horizontal dimension the

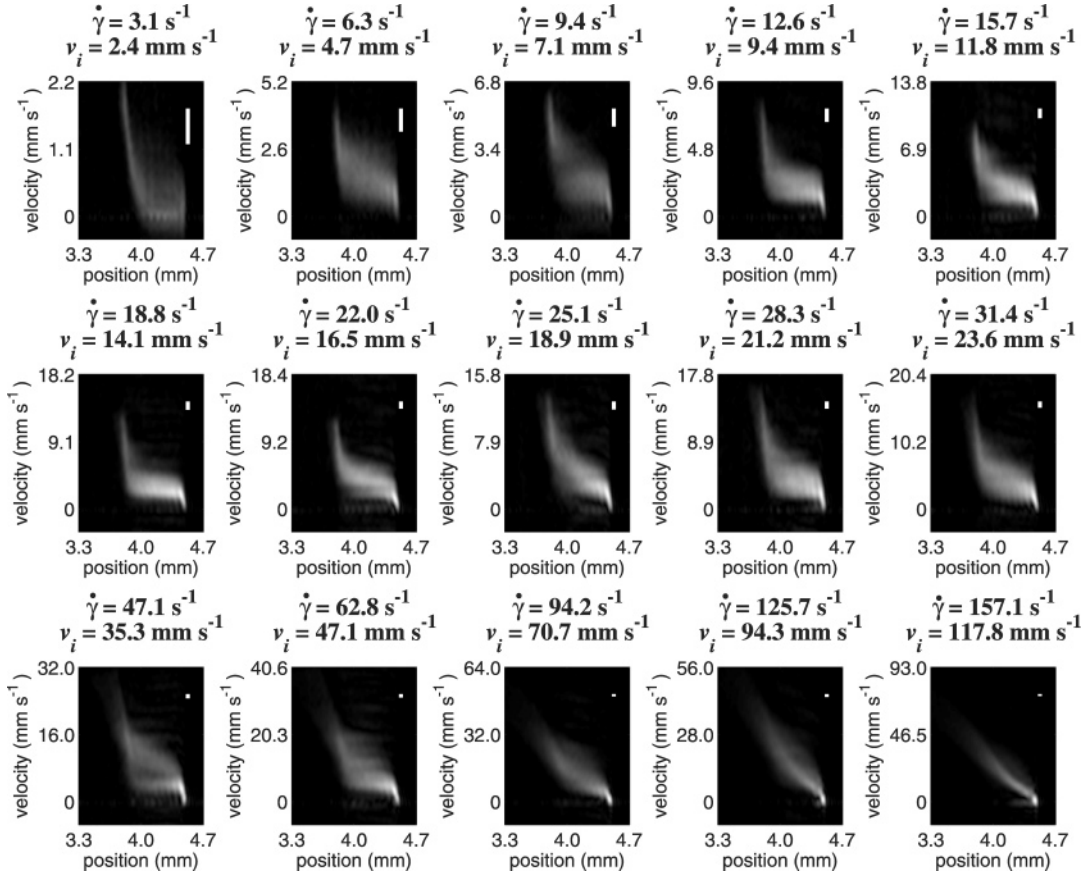

Figure 8. (a) The velocity profiles are shown here at a range of average shear rates at 293 K. The inner wall velocity at corresponding shear rate is indicated, in addition to the distance typically traveled by nuclei undergoing purely diffusive motions.

radial dimension and the vertical dimension the ^{2}H NMR frequency, with spectra from the radial slices nearest the inner and outer walls shown above. The results are quite remarkable and counterintuitive, given the common presumptions about shear-banded flow. Several researchers have argued that shear banding in WLMs is associated with nematic ordering. However the rheo-NMR experiments of Figures 8 and 9 show that such a simple correspondence does not exist.

Indeed, those cases where shear banding occurs, as evidenced by velocimetry, are associated with lack of observed molecular ordering. By contrast, where apparent Newtonian flow is present, strong ordering effects also appear.

VI. Discussion of Models of Phase Behavior

Clearly, more than one physical feature of our WLM system is driving the observations in our array of rheo-NMR experiments. Indeed, this is precisely why the term "complex fluid" applies to WLMs. In contrast to simple linear polymer solutions, WLMs form a "living" system where these supramolecular worms can break and can recombine with each other. They might also form more complex phases such as branched WLMs, vesicles, lyotropic lamellar phases, spherical micelles, or some combination of these possibilities. Similar to linear polymers, WLMs can entangle and can align with each other, and might form a nematic phase in a shear field. Anisotropic alignment may also act in a different way on these materials due to the different nature of stiffness along their axes. The concept of entanglement may differ substantially from that in linear, covalently bound, polymers in that when a worm tube encounters a topological constraint (another tube), it may join with it, or break, or pass through it with some characteristic time scale, possibly depending on shear rate. Our data show several phenomena that narrow the scope of possibilities for the phase behavior of these systems.

The local minima in the temperature dependence of apparent viscosity at high rates (Figure 4a) is highly unexpected, as the worms likely grow the longest at these intermediate temperatures. With very long worms, two possible mechanisms come to mind for explaining the viscosity reduction at high shear rates. Have the WLMs grown long enough to flow-align and form a nematic phase at high rates? Or perhaps when long enough, the WLMs can break in shear to lower their viscosity. The temperature dependent ^{2}H NMR splitting in Figure 6 can distinguish between these two viscosity reduction mechanisms. If a nematic phase formed at 294 K, we would expect to see an enhanced splitting. Instead the inner splitting disappears completely, suggesting that shear simply breaks the WLMs at high shear rates near 294 K.

On first inspection, we supposed that the two ^{2}H NMR splittings seen in the spectra of Figure 6 might be due to one of the following three hypotheses: (1) the two distinct ^{2}H sites (in terms of CD bond angle with respect to B_0) on the phenylethanol molecule, if it were ordered along a well-defined axis, or (2) the probe molecule could be partitioning between two parts of the worms, for example the core and corona, or (3) the probe molecule could be partitioning between different phases or domains. On close inspection, hypothesis 1 does not fit the data in that if it were true, the two pairs of lines would have exactly the same (proportional) dependence of splitting on temperature, and their linewidths would also have the same dependence. Hypothesis 2 seems far more likely. Indeed SANS data suggest that, while the phenylethanol prefers the core

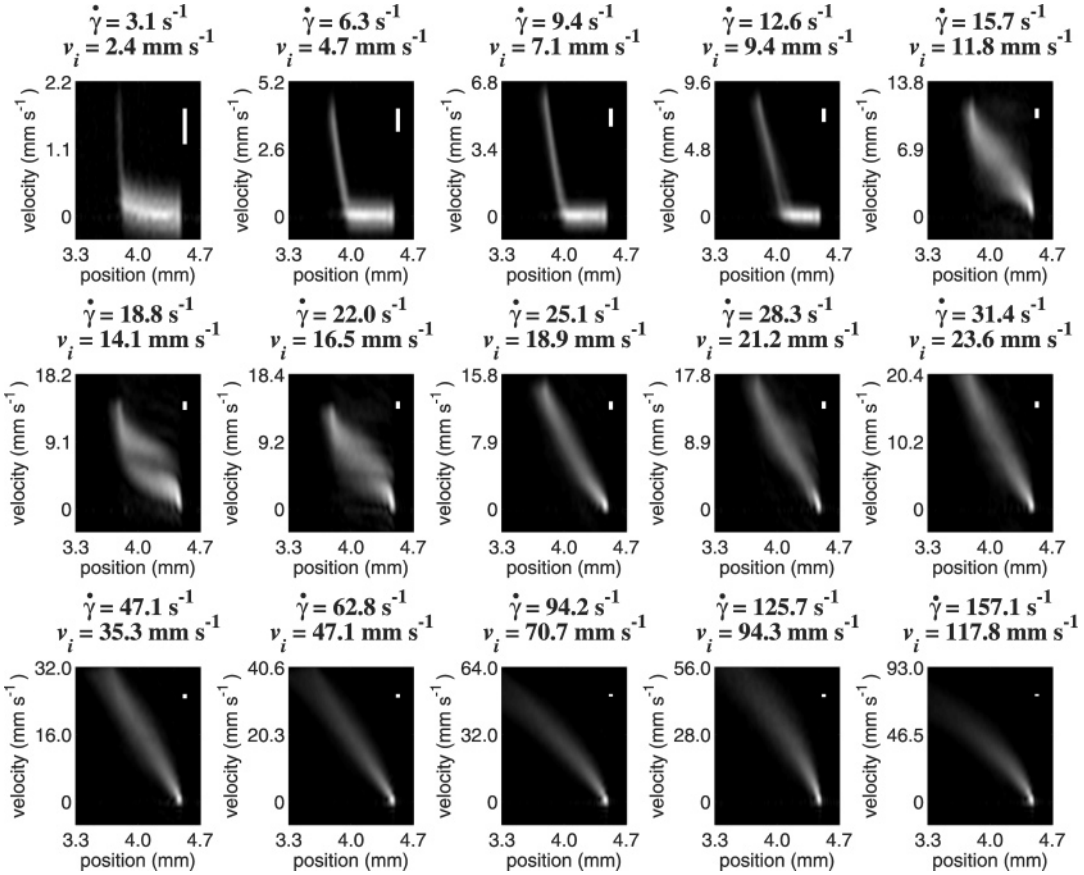

Figure 9. (a) Velocity profiles shown here at a range of average shear rates at 304 K. The inner wall velocity at corresponding shear rate is indicated, in addition to the distance typically traveled by nuclei undergoing purely diffusive motions.

(hydrogen bonded to the ether oxygen of PPO), it also exists in the corona[13] (hydrogen bonded to the ether oxygen of PEO). However, the diffusion coefficient of the probe molecule (see Figure 5), $D \approx 3 \times 10^{-10}\ m^2\ s^{-1}$, means that the probe molecule diffuses approximately $\sqrt{6Dt} \approx 10\ \mu m$ on the time scale of our ^2H NMR spectroscopy experiment ($\sim$0.05 s). This is considerably larger than the core diameter (7 nm) of the worms.[13] We can only explain the Figure 6 data with the idea that the probe molecule must exist in two distinct phases or domains of the system, which are stable at least on the $\sim$0.05 s time scale. Furthermore, examining the Figure 6 data, it is clear that the relative amounts of the two phase or domain types do not change over the observed temperature range of 30 K.

Just as interesting is the complexity in the temporal character of shear rate profiles, as revealed by the time-resolved and steady-state NMR velocimetry. The thixotropy of this micellar system, as seen in the rheological measurements, is also apparent in the time taken to reach a steady-state velocity profile, as evidenced in the data of Figure 7, where a time series of velocity maps for the shear rate, 6.2 s^{-1} at 304 K indicates an initially fluctuating profile, with a steady shear-banded state formed after 600 s.

Remarkably, once this steady state is reached, there is no obvious relationship between shear banding and a state of nematic order. In Figures 10 and 11, obtained at two different temperatures of 293 and 304 K, respectively, no correspondence can be ascertained. At 293 K and 3.1 s^{-1}, we see evidence of nematic order through the split deuterium spectrum in conjunction with a shear banded state, and yet there is no discontinuity of nematic order associated with the discontinuous shear rate. At 304 K, at the same gap averaged rate of 3.1 s^{-1}, as well as

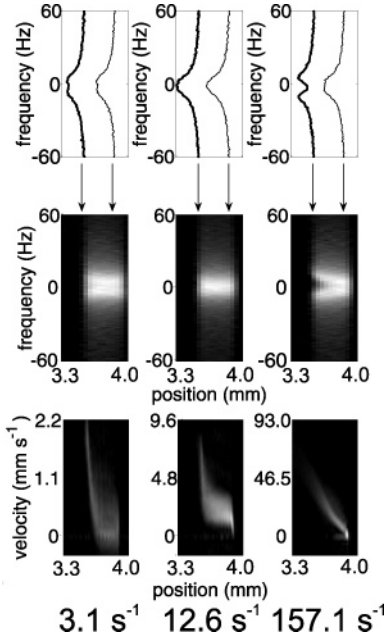

Figure 10. (a) Variation of the velocity profile with shear rate at 293 K. The inner wall velocities for the gap-averaged shear rates of 3.1, 12.6, and 157.1 s^{-1} are 2.4, 9.4, and 117.8 s^{-1}, respectively. The top three panes indicate the NMR spectrum of the sample at the inner and outer walls, as obtained through the radial spectroscopic technique described.

at 12.4 s^{-1} no nematic order is seen at all, despite manifestly shear-banded states. The greatest degree of nematic order is found at 293 K, under conditions where no shear banding is apparent at all. This nematic order varies continuously across

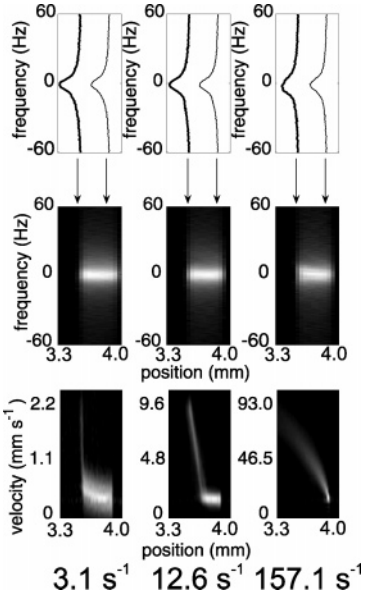

Figure 11. (a) Variation of the velocity profile with shear rate at 304 K. The inner wall velocities for the gap-averaged shear rates of 3.1, 12.6, and 157.1 s^{-1} are 2.4, 9.4, and 117.8 s^{-1}, respectively. The top three panes indicate the NMR spectrum of the sample at the inner and outer walls.

the gap, even though the shear rate appears homogeneous. Finally, in relation to shear rate profiles, both fluctuating and steady profiles are observed, the sweep at 304 K shown in Figure 9 exhibiting transitions from fluctuating to steady to fluctuating as the gap-averaged strain rate is gradually increased.

This bewildering array of phenomenology is more complex than is found in the classical wormlike micellar systems based on ionic amphiphiles, examples being cetylpyridinium chloride/sodium salicylate in water[8] and cetyltrimethylammonium bromide in water.[43] The most noteworthy difference is the strong temperature dependence of and temperature inflection in the viscosity at finite shear rate. Nonetheless, there are some similarities in the lack of clear correspondence between shear bands and nematic ordering,[43] as well as the diversity of fluctuation dynamics[48] which classical ionic surfactant micelles exhibit. We present these data here in order to illustrate the rich diversity of phenomenology that remains to be explained in the rheology of Pluronic surfactant phases.

VII. Conclusions

The rheo-NMR methods presented here combine novel spatially resolved NMR spectroscopy and velocimetry. The high resolution ^{2}H NMR spectroscopic measurements are made possible by the use of Hankel transformation methods which utilize the entire signal from the entire Couette cell annulus. It depends on the use of a deuterated probe molecule, in this case the phenylethanol needed for the micelle formation. The velocimetry data was obtained using a rapid single slice phase-encoding method which permitted velocity profiles at 1 s repetition times. The assignment of peaks in the NMR spectrum has been assisted by the use of spectrally resolved molecular diffusion (DOSY) measurements.

The most significant findings concern (i) a flow curve exhibiting plateau-like properties in the stress with the lower strain rate limit of the plateau at the remarkably small value of $10^{-2}s^{-1}$, (ii) the inflected temperature dependence of the low shear rate viscosity, an effect which correlates with the temperature dependence of the micellar nematic order, (iii) the dual order parameters of the nematic state, as sensed by the deuterated phenylalcohol probe molecule, (iv) the lack of a simple correspondence between shear banding and the spatially dependent order parameter, (v) the bewildering array of spatially dependent shear rates and associated fluctuations, and (vi) the thixotropy as seen in the time dependent stress at fixed shear rate following startup.

We attribute the very low strain rate at the onset of the plateau to slow dissociation/recombination dynamics for these Pluronic micellar systems. The dual order parameters we attribute to partitioning between the micellar corona and core. The fluctuations in shear banding are not by themselves remarkable effects and are now accepted as a fairly universal property of shear banding dynamics in wormlike micelle systems. The lack of a clear correspondence between nematic order and shear banding, something which has been pointed out for a different system of ionic amphiphiles, only serves to emphasize that our models for shear banding and band dependence on molecular organization, are far from understood.

Acknowledgment. R.H.C. is grateful for a Fulbright Senior Scholarship that supported his six month stay in New Zealand in 2005, which started this work. B.S.D. and P.T.C. are grateful to the Royal Society of New Zealand Marsden Fund and Centres of Research Excellence Fund for financial support.

References and Notes

(1) Rehage, R.; Hoffmann, H. *Mol. Phys.* **1991**, *74*, 933.
(2) Khatory, A.; Lequeux, F.; Kern, F.; Candau, S. J. *Langmuir* **1999**, *9*, 1456.
(3) Clausen, T. M.; Vinson, P. K.; Minter, J. R.; Davis, H. T.; Talmon, Y.; Miller, W. G. *J. Phys. Chem.* **1992**, *96*, 474.
(4) Holmberg, K.; Jönsson, B.; Kronberg, B.; Lindman, B. *Surfactants and polymers in aqueous solution*; Wiley, West Sussex, U.K., 2003.
(5) Evans, D. F.; Wennerstrom, H. *The Colloidal Domain: Where Physics, Chemistry, Biology, and Technology Meet* (Advances in Interfacial Engineering) (Hardcover); Wiley-VCH, 1999.
(6) Lequeux, F.; Candau, S. J. Structural properties of Wormlike Micelles. In *Theoretical Challenges in Complex Fluids*; McLeish, T. C. B., Ed.; Nato ASI series, Series E Applied Sciences 339; Kluwer: Boston, MA, 1996.
(7) Cappelaere, E.; Berret, J-F.; Decruppe, J. P.; Cressely, R.; Lindner, P. *Phys. Rev. E* **1997**, *56*, 1869.
(8) Rehage, H.; Hoffman, H. *J. Phys. Chem.* **1988**, *92*, 4712.
(9) Appell, J.; Porte, G.; Khatory, A.; Kern, F.; Candau, S. J. *J. Phys. II* **1992**, *2*, 1045.
(10) BASF Corp. *Pluronic and Technical Brochure Tetronic Surfactants*; BASF: Parispanny, NJ, 1989.
(11) Alexandridis, P.; Hatton, T. A. *Colloids Surf. A* **1995**, *96* 1.
(12) Chu, B. *Langmuir* **1995**, *11*, 414.
(13) Guo, L.; Colby, R. H.; Thiyagarajan, P. *Physica B* **2006**, *685*, 385−6.
(14) Cates, M. E.; Candau, S. J. *J. Phys. Condens. Matter* **1990**, *2*, 6869.
(15) Berret, J-F.; Roux, D. C. *J. Rheol.* **1995**, *39*, 725.
(16) Cates, M. E.; McLeish, T. C. B.; Marrucci, G. *Europhys. Lett.* **1993**, *21*, 451.
(17) Decruppe, J. P.; Cressely, R.; Makhloufi, R.; Cappelaere, E. *Colloid Polym. Sci.* **1995**, *273*, 346.
(18) Makhloufi, R.; Decruppe, J. P.; Ait-Ali, A.; Cressely, R. *Europhys. Lett.* **1995**, *32*, 253.
(19) Callaghan, P. T.; Cates, M. E.; Rofe, C. J.; Smeulders, J. B. A. F. *J. Phys. II France* **1996**, *6*, 375.
(20) Mair, R. W.; Callaghan, P. T. *Europhys. Lett.* **1996**, *36*, 719.
(21) Doi, M.; Edwards, S. F. *The Theory of Polymer Dynamics*; Oxford University Press: Oxford, U.K., 1987.
(22) McLeish, T. C. B.; Ball, R. C. *J. Polym. Sci.* **1986**, *24*, 1735.
(23) Spenley, N. A.; Cates, M. E.; McLeish, T. C. B. *Phys. Rev. Lett.* **1993**, *71*, 939.
(24) Spenley, N. A.; Yuan, X. F.; Cates, M. E. *J. Phys. II* **1996**, *6*, 551.
(25) Berret, J-F.; Roux, D. C.; Porte, G. *J. Phys. II Fr.* **1994**, *4*, 1261.
(26) Cates, M. E. *Macromolecules* **1987**, *20*, 2289.
(27) Cates, M. E. *J. Phys. Fr.* **1988**, *49*, 1593.
(28) Cates, M. E. *J. Phys. Chem.* **1990**, *94*, 371.
(29) Mair, R. W.; Callaghan, P. T. *J. Rheol.* **1997**, *41*, 901.
(30) Britton, M. M.; Callaghan, P. T. *J. Rheol.* **1997**, *41*, 1365.

(31) Méndez-Sánchez, A. F.; López-González, M. R.; Rolón-Garrido, V. H.; Pérez-González, J.; de Vargas, L. *Rheol. Acta* **2003**, *42*, 56.
(32) Salmon, J-B.; Colin, A.; Manneville, S.; Molino, F. *Phys. Rev. Lett.* **2003**, *90*, 228303.
(33) Salmon, J-B.; Becu, L.; Manneville, S.; Colin, A. *Eur. Phys. J. E* **2003**, *10*, 209.
(34) Salmon, J-B.; Becu, L.; Manneville, S.; Colin, A. *Phys. Rev. E* **2003**, *68*, 051503.
(35) Salmon, J-B.; Becu, L.; Manneville, S.; Colin, A. *Phys. Rev. E* **2003**, *68*, 051504.
(36) Manneville, S.; Salmon, J-B.; Colin, A. *Eur. Phys. J. E* **2004**, *13*, 197.
(37) Manneville, S.; Becu, L.; Colin, A. *Eur. Phys. J., Appl. Phys.* **2004**, *28* (3), 361.
(38) Becu, L.; Manneville, S.; Colin, A. *Phys. Rev. Lett.* **2004**, *93*, 018301.
(39) Fischer, E.; Callaghan, P. T. *Phys. Rev. E* **2001**, *6401*, 1501.
(40) Schmidt, V.; Lequeux, F.; Pusse, A.; Roux, D. *Langmuir* **1994**, *10*, 955.
(41) Wheeler, E. K.; Fischer, P.; Fuller, G. G. *J. Non-Newtonian Fluids Mech.* **1998**, *75*, 193.
(42) Fischer, P. *Rheol. Acta* **2000**, *39*, 234.
(43) Fischer, P.; Wheeler, E. K.; Fuller, G. G. *Rheol. Acta* **2001**, *41*, 35.
(44) Hu, Y.; Wang, S. Q.; Jamieson, A. M. *J. Rheol.* **1993**, *37*, 531.
(45) Hu, Y.; Matthys, E. F. *Rheol. Acta* **1995**, *34*, 450.
(46) Bandyopadhyay, R.; Basappa, G.; Sood, A. K. *Phys. Rev. Lett.* **2000**, *84*, 2022.
(47) Holmes, W. M.; López-González, M. R.; Callaghan, P. T. *Eur. Phys. Lett* **2003**, *64*, 274.
(48) López-González, M. R.; Photinos, P.; Holmes, W. M.; Callaghan, P. T. *Phys. Rev. Lett.* **2004**, *93*, 268302.
(49) Britton, M. M.; Callaghan, P. T. *Eur. Phys. J.* **1999**, *B7*, 237.
(50) Fielding, S. M.; Olmsted, P. D. *Phys. Rev. Lett.* **2004**, *92*, 084502.
(51) Fielding, S. M.; Olmsted, P. D. *Eur. Phys. J. E* **2003**, *11*, 65.
(52) Nakatani, A. I.; Poliks, M. D.; Samulski, E. T. *Macromolecules* **1990**, *23*, 2686.
(53) Siebert, H.; Grabowski, D. A.; Schmidt, C. *Rheol. Acta* **1997**, *36*, 618.
(54) Callaghan, P. T. *Principles of Nuclear Magnetic Resonance Microscopy*, Oxford University Press: Oxford, U.K., 1991.
(55) Callaghan, P. T. *Rep. Prog. Phys.* **1999**, *62*, 599.
(56) Callaghan, P. T. *Curr. Opin. Colloid Sci.* **2006**, *11*, 13.
(57) Slichter, C. P. *Principles of Magnetic Resonance*; Springer: New York, 1996.
(58) Seelig, A.; Seelig, J. *Biochemistry* **1974**, *13*, 4839.
(59) Lafleur, M.; Bloom, M.; Elkenburry, E. F.; Gruner, S.; Han, Y.; Cullis, P. *Biophys. J.* **1996**, *70*, 2747.
(60) Luz, Z.; Meiboom, S. *J. Chem. Phys.* **1973**, *59*, 275.
(61) Callaghan, P. T.; Kilfoil, M. L.; Samulski, E. T. *Phys. Rev. Lett.* **1998**, 814524.
(62) Kilfoil, M. L.; Callaghan, P. T. *Macromolecules* **2000**, *33*, 6828.
(63) Callaghan, P. T.; Samulski, E. T. *Macromolecules* **2003**, *36*, 724.
(64) Bodenhausen, G.; Vold, R. R.; Vold, R. J. *J. Magn. Reson.* **1980**, *37*, 93.
(65) Stejskal, E. O.; Tanner, J. E. *J. Chem. Phys.* **1965**, *42*, 288.
(66) Morris, K. F.; Johnson, C. S. *J. Am. Chem. Soc.* **1993**, *115*, 4291.
(67) Won, Y-Y.; Davis, H. T.; Bates, F. S. *Science* **1999**, *283*, 960.
(68) Waton, G.; Michels, B.; Steyer, A.; Schosseler, F. *Macromolecules* **2004**, *37*, 2313.
(69) Duval, M.; Waton, G.; Schosseler, F. *Langmuir* **2005**, *21*, 4904.
(70) Castelletto, V.; Hamley, I. W. *Polym. Adv. Technol.* **2006**, *17*, 137.
(71) Guo, L.; Colby, R. H.; Lin, M. Y.; Dado, G. P. *J. Rheol.* **2001**, *45* (5), 1223.
(72) Cates, M. E.; Fielding, S. M. *Adv. Phys.* **2006**, *55* (7−8), 799.
(73) Berret, J.-F. In *Molecular Gels*; IWeiss, R. G., Terech, P., Eds.; Elsevier: Amsterdam, 2005.
(74) López-González, M. R.; Holmes, W. M.; Callaghan, P. T. *Soft Matter* **2006**, *2*, 855.

MA071807F